Flow tube studies of the C(3P) reactions with ethylene and propylene

Michael Capron, Jérémy Bourgalais, Ranjith Kumar Abhinavam Kailasanathan, David L. Osborn, Sébastien D. Le Picard, Fabien Goulay

Flow tube studies of the C(^{3}P) reactions with ethylene and propylene

Michael Capron,[1] Jérémy Bourgalais,[1] Ranjith Kumar Abhinavam Kailasanathan,[2] David L. Osborn,[3] Sébastien D. Le Picard,[1,] Fabien Goulay[2,*]*

[1] Institut de Physique de Rennes, Département de Physique Moléculaire, Astrophysique de Laboratoire, UMR CNRS 6251, Université de Rennes 1, Campus de Beaulieu, 35042 Rennes Cedex, France

[2] Department of Chemistry, West Virginia University, Morgantown, West Virginia 26506, USA

[3] Combustion Research Facility, Mail Stop 9055, Sandia National Laboratories, Livermore, California 94551, USA

[*]Electronic mail: sebastien.le-picard@univ-rennes1.fr, fabien.goulay@mail.wvu.edu

ABSTRACT

Product detection studies of C(^{3}P) atom reactions with ethylene, $C_2H_4(X^1A_g)$ and propylene, $C_3H_6(X^1A')$ are carried out in a flow tube reactor at 332 K and 4 torr (553.3 Pa) under multiple collision conditions. Ground state carbon atoms are generated by 193-nm laser photolysis of carbon suboxide, C_3O_2 in a buffer of helium. Thermalized reaction products are detected using tunable VUV photoionization and time of flight mass spectrometry. For C(^{3}P) + ethylene, propargyl (C_3H_3) is detected as the only molecular product in agreement with previous studies on this reaction. The temporal profiles of the detected ions are used to discriminate C(^{3}P) reaction products from side reaction products. For C(^{3}P) + propylene, two reaction channels are identified through the detection of methyl (CH_3) and propargyl (C_3H_3) radicals for the first channel and C_4H_5 for the second one. Franck-Condon Factor simulations are employed to infer the C_4H_5-isomer distribution. The measured 1:4 ratio for the *i*-C_4H_5 isomer relative to the methylpropargyl isomers is similar to the C_4H_5 isomer distribution observed in low-pressure flames and differs from crossed molecular beams data. The accuracy of these isomer distributions is discussed in view of large uncertainties on the photoionization spectra of the pure C_4H_5 isomers.

Introduction

The chemistry of carbon atoms is involved in a wide variety of environments, from combustion reactors to astrophysical objects. Atomic carbon, the fourth most abundant element in the Universe, is ubiquitous in the interstellar medium and has been observed in various astronomical objects.[1-3] In combustion flames, although their detection is experimentally very challenging,[4] their reaction was proposed to be responsible for C_2 formation and chemiluminescence.[5] Carbon atoms have been detected in discharge plasmas,[6] chemical vapor deposition processes,[7] and are also abundant in thermal plasmas.[8] In all these environments the reactions of carbon atoms with small hydrocarbons are believed to initiate complex radical chemical schemes leading to the formation of larger molecules.[6,9] Reactions of ground-state atomic carbon $C(^3P)$ with unsaturated hydrocarbons and free radicals are therefore important in order to better understand and predict the growth of carbon containing molecules, including the formation of polycyclic aromatic hydrocarbons (PAHs).

Pioneering kinetic measurements performed by Husain and Haider[10,11] demonstrated that $C(^3P)$ reactions with hydrocarbons are very fast at room temperature. Very low temperature kinetic experiments (down to 20 K) also showed that these reactions remain rapid at low collision energies, indicating the absence of a barrier in the entrance channel.[12-14] Even in cold environments such as interstellar clouds or planetary atmospheres, $C(^3P)$ atoms will significantly contribute to the chemistry by fast barrierless reactions with the abundant hydrocarbons.[12,15]

Reactions of ground state carbon atoms with small hydrocarbons are predicted to proceed by addition of the carbon atom onto carbon double or triple bonds to form an energy-rich reaction adduct.[15] Large uncertainties still remain regarding the fate of the so-formed intermediate. One of the proposed exit channels used in chemical models is the loss of a hydrogen atom to form larger open-shell hydrocarbons. The overall reaction can be written as $C + C_nH_m \rightarrow C_{n+1}H_{m-1} + H$. H-atom branching ratios for $C(^3P)$ reactions with unsaturated hydrocarbons have been studied by Bergeat and Loison.[16,17] In most cases, the

H-loss accounts for no more than half of the reaction products. This result may be explained by competitive C-H and C-C cleavage as well as by the transition of the reaction intermediate from the triplet surface to the singlet surface by intersystem crossing (ISC).[18] The accuracy of the models reproducing the chemistry of carbon-rich environments strongly depends on the identification of all the reaction products.

In addition to H-atom detection in flow reactors,[16,17] crossed molecular-beams experiments combined with theoretical calculations have been widely used to investigate the dynamics of carbon atoms with a variety of hydrocarbons. The product formation of the reaction $C(^3P)$ + ethylene (C_2H_4) was successively studied by R. Kaiser and co-workers at 7.1 and 38.1 kJ mol^{-1} collision energies,[19] by M. Costes, P. Casavecchia and co-workers at collision energies ranging from 0.49 to 30.8 kJ mol^{-1} [14] and more recently by S.-H. Lee and co-workers at 14.6 kJ mol^{-1}.[20] In these crossed beams experiments the products are detected by laser induced fluorescence of H-atoms,[14] or quadrupole mass spectrometry coupled to electron impact ionization[14,19] or synchrotron radiation photoionization.[20] *Ab initio* calculations by Mebel and co-workers[21] indicate that the $C(^3P) + C_2H_4$ reaction proceeds without an entrance barrier, as confirmed by the low temperature experimental kinetic study of Chastaing et al.[12] Theoretical investigations of the C_3H_4 potential energy surface have shown the presence of many minima on the potential energy surface leading to various isomers with a large number of energetically allowed dissociation routes.[22,23] Mebel and co-workers performed Rice-Ramsperger-Kassel-Marcus (RRKM) calculations for collision energies lower than 38.5 kJ mol^{-1} resulting in branching ratios of 98-99% for the H_2CCCH + H channel, 1-2% for the CH_2 + C_2H_2 channel, and negligible contributions from other channels.[22] These single collision branching ratios are consistent with the kinetic study of Bergeat et al.[16] performed at room temperature (ca. 4 kJ mol^{-1}) and 2 Torr in a flow reactor showing an absolute H-branching ratio of 0.92 ± 0.04 under multiple collision conditions. The works of Kaiser and co-workers and Casavecchia and co-workers also led to the conclusion that C_3H_3 (propargyl) + H was the main channel of the $C(^3P) + C_2H_4$ reaction. However, at collision energies greater than 6 kJ mol^{-1}, Casavecchia and co-workers claimed the presence of at least one other H-atom elimination channel forming a less

stable C_3H_3 isomer(s). In the most recent study, Chin et al.[20] investigated the velocity distribution of C_3H_3 radicals produced by the $C(^3P)$ + C_2H_4 reaction, at 14.6 kJ mol^{-1} collision energy, using two different photoionization energies: 9.5 and 11.6 eV. For both ionization energies, the time of flight remains unchanged, indicating that only one isomer contributed to the C_3H_3 isomer channel, which was identified as propargyl (H_2CCCH) based on its photoionization spectrum.

The product formation of the $C(^3P)$ + propylene (C_3H_6) reaction was first studied by Kaiser and co-workers[24] who recorded product angular and velocity distributions of C_4H_5 radical at m/z=53 at average collision energies of 23.3 and 45.0 kJ mol^{-1}. Similar to the $C(^3P)$ + ethylene reaction, low temperature experimental kinetic studies[25] and ab initio calculations performed by Mebel and co-workers[21] demonstrated that the carbon atom is likely to add to the π-orbitals of propylene without an entrance barrier. More recently, Lee and co-workers[26] identified C_4H_5 + H, C_4H_4 + 2H and C_3H_3 + CH_3 as exit channels in $C(^3P)$ + propylene in their crossed molecular beams experiment coupled to synchrotron radiation mass spectrometry. Quantum calculations were used to calculate the C_4H_6 potential energy surface and infer the most likely reaction mechanisms.[21,24-26] The accepted mechanism is the addition of the triplet carbon onto the reactant double bond to form a cyclic intermediate with no activation energy. The reaction adduct then isomerizes via ring opening to give the triplet *Z*- and *E*-CH_3CHCCH_2 stereoisomers.[24,26] These triplet C_4H_6 adducts are found to isomerize through H-atom transfer and to decompose through H-loss to form $H_2CCCHCH_2$ (*i*-C_4H_5), $HCCCHCH_3$ and H_2CCCCH_3, two methylpropargyl isomers. The CH_3 + C_3H_3 (propargyl) channel is also found to be energetically accessible. All the transition states are found to be below the energy of the reactants.

RRKM calculations on these surfaces predict branching ratios for $HCCCHCH_3$/H_2CCCCH_3/i-C_4H_5 + H and H_2CCCH + CH_3 of 7:5:10:78 respectively at 17 kJ mol^{-1}, while experimental evaluations based on ionization efficiencies give a ratio of 17:8:75 for the C_4H_5 (sum of all isomers):C_4H_4:C_3H_3 products.[26] The same authors used photoionization spectroscopy of C_4H_5 (m/z=53) at photon energies ranging from 7

to 12 eV to assign $HCCCHCH_3$, H_2CCCCH_3 and *i*-C_4H_5 as the main formed isomers at 16 kJ mol^{-1} collision energy. They determined the yield of the sum of the $HCCCHCH_3$ and H_2CCCCH_3 relatively to the *i*-C_4H_5 contributions to be ~1.4 by fitting calculated photoionization spectra to the experimental data assuming all isomers have identical photoionization cross sections.

A better understanding of the role of $C(^3P)$ chemistry in interstellar chemistry, combustion and plasma environments requires probing its reaction mechanisms with hydrocarbons over a very wide range of experimental conditions, including multiple collision environments. In this study, we present the detection of the products formed by the reactions of carbon atoms with ethylene and propylene under multiple collision conditions at 332 K and 4 Torr and compare the results to recent crossed molecular-beams data. Flow tube and crossed beams experiments differ significantly by the energy range and the collisional conditions. Crossed beam experiments look at the formation and dissociation of reaction intermediates following a single collision of the reactants with no effect from the surrounding environment. In flow tube experiments the large number of collisions leads to the thermalization of the products to the temperature of the flow and may induce, in some cases, stabilization of reaction adducts and intermediates. Flow tube experiments have been applied to a wide variety of reactions, and are complementary to crossed molecular beam experiments; each approach has its advantages and disadvantages. For example, crossed beam experiments can be quite sensitive to heavy/light product channels (when probing the heavy product that is confined to a small Newton sphere), but much less sensitive to highly exothermic bimolecular channels with more even mass pairs. This bias doesn't exist in a collisional experiment. Angular distributions can be easily extracted from crossed molecular beam experiments, and generally not possible to extract from collisional environments. Photoionization spectra are less often acquired in crossed beam environments because the signal levels can make this challenging, whereas such spectra for identifying isomers are routine in flow tube experiments. Numerous studies have been performed using flow tube[27-32] and crossed molecular beams,[14,33-38] the combination of which has provided very valuable information for the understanding of the chemistry of gas phase environments

ranging from the interstellar medium to combustion flames. However, it is important to note that flow tube experiments are able to provide information about bimolecular processes only if one can discriminate between primary and secondary processes as well as demonstrate that the relevant products are formed by the studied reactions. Previous studies for highly reactive radicals (C_2H, CH, CN) have demonstrated that the time-, mass-, and energy-resolved detection of the products makes such identification possible.[27,28,39-43] Goulay et al.[39] have demonstrated that multiplex photoionization mass spectrometry can directly rule out multiple collision effects when they do not happen.

In the present study, carbon atoms are created from photodissociation of carbon suboxide, C_3O_2, at 193 nm, and are shown to be formed essentially in their ground electronic state, $C(^3P)$, eliminating the effect of $C(^1D)$ reactions. The products of both reactions are detected using time-resolved mass spectrometry combined with synchrotron photoionization spectroscopy. The effect of secondary reactions and pressure on the product distribution is discussed as well as the relevance of the experimental data for carbon-rich gas phase environments.

Experimental section

The reactions are performed in a slow flow reactor coupled to a time-resolved photoionization time of fight mass spectrometer at the Advanced Light Source (ALS) synchrotron at the Lawrence Berkeley National Laboratory. A description of the apparatus has been given elsewhere[32,44] and only a brief overview is presented here. The flow tube is a 62-cm long quartz tube with 1.05 cm inner diameter. The gas pressure within the reaction tube is typically 4 Torr (533.3 Pa) with a total gas flow of 250 sccm (standard cubic centimetres per second). All the experiments are performed at 332 K corresponding to a gas flow velocity of 11 m s^{-1} and total number density of 1.16×10^{17} cm^{-3}. The helium buffer gas, carbon atom precursor (C_3O_2, 1.40×10^{14} cm^{-3}) and reaction gases (ethylene, 2.55×10^{14} cm^{-3}, and propylene 2.32×10^{14} cm^{-3}) are supplied to the reaction flow via separate mass-flow controllers. The pressure within the reaction flow-tube is maintained constant using a butterfly valve that throttles a roots pump. Carbon

atom reactions are initiated by 193 nm photolysis of carbon suboxide, C_3O_2, using a pulsed excimer (ArF) laser operating at 10 Hz.

C_3O_2 is synthesized prior to the experiments via the dehydration of bis(trimethylsilyl) malonate (BTSM, Aldrich, 98% purity) using variations to the procedure reported by Birkoger and Sommer (with a 54% C_3O_2 yield).[45] The system consists of a 3-neck flask (250 mL) connected to a nitrogen purge, two glass traps in series and a mechanical pump. The pressure in the entire system is measured using an absolute pressure gauge. The system is flushed with dry nitrogen at atmospheric pressure for at least 3 hours to remove any residual water. About 40 g phosphorous pentoxide (P_2O_5, Aldrich, 98.5% purity) is mixed with 20 g sand and placed in the flask. The phosphorous pentoxide is flushed with dry nitrogen to remove water. The system (flask and traps) is then evacuated to a pressure below 10 torr using a mechanical pump. About 20 mL of BTSM is measured with a syringe and injected at once through a rubber septum into the 3-neck flask. The reaction occurs spontaneously leading to a dark-red coloration of the solid and production of gas. The mixture of gaseous products is collected at 77 K in a large glass bubbler. After complete stop of gas production (formation of gas bubbles in the reactant flask) (~40 min) the liquid nitrogen is replaced by an acetone-liquid nitrogen slush at 179 K and the bubbler is evacuated. At this temperature, C_3O_2 has a negligible vapor pressure while CO_2 sublimes rapidly, leaving behind only C_3O_2 in the trap. Up to 110 Torr of C_3O_2 is then collected and buffered with 1100 Torr of helium in a 3.79 L stainless steel cylinder. The photoionization spectra of the gas mixture at m/z=68 confirmed the formation of carbon suboxide (Ionization Energy, IE=10.6 eV).[46]

The 193-nm laser fluence inside the reaction flow tube ranges from 20 to 50 mJ/cm^2. Initial carbon atom number density in the flow tube is estimated to be approximately 2×10^{11} cm^{-3}. At ~30 cm along the flow tube, a 650 μm diameter pinhole allows a small portion of the gas mixture to escape into a vacuum chamber. This gas is sampled by a skimmer creating a beam of molecules that is subsequently intersected by the quasi-continuous vacuum-ultraviolet (VUV) synchrotron radiation. Ions formed in this region are

detected as a function of their mass-to-charge (m/z) ratio using a 50 kHz pulsed orthogonal-acceleration time-of-flight mass spectrometer. All detected ions are time-tagged relative to the excimer laser pulse (at t = 0) and accumulated in a multichannel scaler. In this way, complete mass spectra are collected as a function of reaction time. The excimer laser is operated at 10 Hz, allowing sufficient time between laser pulses to completely refresh the gas mixture before the next laser pulse. The total ion detection time-window is 50 ms, beginning 10 ms before the laser pulse.

Reagent gases were used without further purification: ethylene (99.9%, Aldrich), propylene (>99%, Aldrich).

Computational methods

C_4H_5 photoionization spectra are simulated within the Franck–Condon (FC) approximation. Electronic structure calculations of the neutral C_4H_5 species and their cations are carried out using the Gaussian09 package[47] using the B3LYP/CBSB7 method to obtain optimized geometries and Cartesian force constants. All the vibrational frequencies are real, indicating that the optimized geometries represent minima on the potential energy surface. The FC factors are calculated at 298 K using the G09 package within the Franck–Condon approximation.[48] The simulated factors are convolved with a 40 meV (FWHM) Gaussian response function and integrated to simulate photoionization spectra. The spectra are shifted such that the energy difference between the neutral and ion ground states matches the ionization energy calculated by Hansen et al. using B3LYP/6–311++G(d,p) level of theory.[49]

Results and discussion

At 4 Torr and 332 K the collision frequency of the products (for example C_3H_3) with the He buffer gas is of the order of 17×10^6 s^{-1} (or 1 collision every 59 ns). Under these conditions, the products are rapidly thermalized to the flow temperature. These collisions may also stabilize reactive intermediates if the unimolecular decay of such chemically activated intermediates occurs on the same timescales (0.1 – 200

microseconds) as collisional energy transfer. For unimolecular decay rates faster than ~ 17×10^{6} s^{-1}, stabilization cannot compete with dissociation, and chemically activated intermediates will decay in the same way as in crossed molecular beams experiments. Therefore, when a reactive intermediates decays with a lifetime shorter than the collision frequency, and it decays to a stable molecule with a lifetime much longer than the collision frequency, the product branching observed via crossed molecular beams and collisional experiments should be identical if the proper weighting is given to the range of collision energies.

Successive reactions of the formed products with other radicals present in the reaction flow may also occur over a short time scale (<1 ms). These reactions will lead to secondary products at higher molecular masses than that of the $C(^3P)$ + hydrocarbons products. At 193 nm, hydrocarbon photodissociation cross sections are relatively high leading to a large number of side reactions. Because $C(^3P)$ reactions are very fast, under the experimental conditions, they will occur within few hundreds of microseconds after the laser pulse. It is therefore possible to discriminate between $C(^3P)$ reaction and slower reactions by inspecting the product time traces. In the following sections, the contribution from slow reactions ($k_{2nd}<5\times10^{-12}$ cm^3 $molec^{-1}$ s^{-1} or $k_{1st}<500$ s^{-1}) or subsequent reactions is minimized by integrating mass spectra only over the 0–1ms time range.

Time- and energy-resolved mass spectra are obtained by averaging at least 500 laser shots at each photon energy. In the present study the ionizing photon energy is scanned from 7.4 to 10.6 eV in steps of 0.025 eV. Kr or Ar is used in a gas filter to absorb higher energy photons at harmonics of the undulator energy. All data are normalized to account for the variations in ALS photocurrent using a NIST-calibrated photodiode (SXUV-100, International Radiation Detectors, Inc.). At each mass-to-charge (m/z) ratio, the average signal present before the laser pulse is subtracted from the time dependent data. Mass spectra of the buffer gas with the reactants and/or $C(^3P)$ precursor were recorded at the beginning of each run with and without the laser pulse. No ion signals were detected at m/z=39 and 53, the masses of the expected

$C(^3P)$ + hydrocarbon products. The photoionization spectra at a given m/z ratio are obtained by integrating the data set over the desired mass and time windows. Three independent datasets are recorded for each reaction and averaged. The error bars for a given data point of a photoionization spectrum are twice the standard deviation around the mean value. The photon energy resolution is determined to be of the order of 40 meV by measuring an atomic resonance of Xe.

In the present experiments, carbon suboxide was used as the precursor of ground state carbon atoms, $C(^3P)$, and was chosen to avoid any contribution from the $C(^1D)$ state. The photodissociation of C_3O_2 has been studied by several authors.[50-55] The absorption cross section of carbon suboxide at 193 nm is ca. 10^{-18} cm^2 [56] and the energetically accessible primary product channels are CO + C_2O and $C(^3P)$ + 2CO.[54] The first experimental measurement of the relative yield of carbon atoms to C_2O following the photolysis of C_3O_2 at 193 nm was performed in 1989 by McFarlane et al.[53] Dissociation to CO + C_2O was shown to be the dominant pathway, with a ratio of ground state carbon atoms, $C(^3P)$, to C_2O of 0.06 ± 0.03. Carbon suboxide photolysis at 193 nm has been used by several authors to generate carbon atoms in their ground state. Chastaing et al.[12,13,57] performed kinetics experiments of $C(^3P)$ atom reactions at low temperatures using carbon suboxide as a precursor and monitoring ground state carbon atoms by VUV LIF at ca. 166 nm.

The 193-nm C_3O_2 photodissociation spin allowed exit channel leads to the formation of the singlet $C_2O(\tilde{a}\ ^1\Delta)$ and $CO(X^1\Sigma^+)$.[51,58] Figure 1 shows (a) the mass spectrum and (b) the kinetic trace of C_2O at m/z=40 recorded at 11.3 eV upon irradiation of C_3O_2 in helium. A positive peak represents species production following laser irradiation; a negative peak represents laser-induced destruction. Negative signals at m/z=43 and 60 are likely due to photolysis and dissociative ionization of impurities. The positive signal at m/z=52 could be due to reaction of C_2O with impurities. In the absence of any other reactants, loss on the reactor walls of singlet C_2O, along with its reaction with C_3O_2, is likely to account for the fast signal decay. The most thermodynamically favorable C_2O + C_3O_2 exit channel is the formation

of C_2 and 3CO. In the presence of ethylene and propylene, C_2O is likely to react with the unsaturated molecules via addition followed by CO-loss. C_2O may also react with atomic hydrogen with a rate of 3×10^{-11} cm^3 s^{-1},[59] leading to the formation of CH + CO. In our reaction flow, H atoms are formed from photolysis of the hydrocarbons as well as from their reactions with carbon atoms. Because C_2O is the most abundant radical in the reaction flow, a non-negligible amount of CH radicals will be formed. A list of the main reactions expected to occur upon irradiation of a C_3O_2 in the presence of hydrocarbon reactants at 193 nm is presented in supplementary information.

In the following section, we analyze mass spectra and photoionization spectra obtained upon irradiation of a mixture of carbon suboxide with ethylene and propylene. The formation of C_3H_3, upon photolysis of C_3O_2 in the presence of C_2H_4 is used to demonstrate the formation of atomic carbon. Energy- and time-resolved mass spectra for the C + C_2H_4 reaction with and without adding a large quantity of molecular hydrogen are used to rule out the formation of the excited singlet state, $C(^1D)$. The time behavior of the ion signal after the laser pulse is used to discriminate between $C(^3P)$ reaction products and products from side reactions. For the $C(^3P)$ + C_3H_6 reaction, the isomeric structures of the reaction products are identified by comparing their photoionization spectra to flame data or to the integrated Franck–Condon factors.

$C(^3P)$ + ethylene

Figure 2 displays the background subtracted photoionization mass spectrum obtained following photolysis of a mixture of C_3O_2 and ethylene in helium. The negative signals at m/z=28, 43 and 58 are due to imperfect subtraction of ion signal from ethylene and acetone impurity. At 193 nm, the absorption cross section of ethylene is of the order of 1×10^{-20} cm^2 and its photodissociation may also contribute to the negative signal at m/z=28.[60] The data are recorded at 10.7 eV photon energy and integrated over the 0–1 ms reaction time window. Over this short reaction window, the main ion signals are detected at m/z=39,

m/z=40. If $C(^1D)$ were produced, its quenching by the helium buffer gas is likely to be very slow. In order to address the possible formation of $C(^1D)$ in our experiments, a time- and energy-resolved mass spectrum was recorded adding at least 10 times more molecular hydrogen in the reaction flow than ethylene reactant. The $C(^1D) + H_2$ reaction rate coefficient has been measured to be $2.0(\pm0.6)\times10^{-10}$ cm^3 $molec^{-1}$ s^{-1} at room temperature[61] while the $C(^3P) + H_2 \rightarrow CH + H$ reaction is endothermic by 96 kJ mol^{-1}.[62] An upper limit of the termolecular rate coefficient for $C(^3P) + H_2 + He$ at 300 K was derived by Husain and Young to be $6.9(\pm1.2)\times10^{-32}$ cm^6 $molec^{-2}$ s^{-1}.[63] Under our experimental conditions the expected pseudo first order rate constants are of the order of 53,550 s^{-1} and 510,550 s^{-1} for $C(^3P) + C_2H_4$ and $C(^1D) + H_2$, respectively.[25,64] Therefore, even if the $C(^1D) + C_2H_4$ reaction has a gas-kinetic rate coefficient, any $C(^1D)$ that might be formed via photolysis of C_3O_2 will be consumed predominantly by reaction with molecular hydrogen. The $C(^1D) + H_2$ reaction produces the CH radical in its electronic ground state, which upon reacting with C_2H_4 forms C_3H_4 isomers.[65,66] If $C(^1D)$ were present in our experiment, adding a large amount of molecular hydrogen in the flow tube would lead to an increase of the C_3H_4 ion signal. Furthermore, $C(^1D) + C_2H_4$ is likely to be a source of C_3H_3 and the competitive reaction with H_2 should greatly decrease the amount of C_3H_3 formed by the $C(^1D)$ + ethylene reaction. However, the absolute intensities of m/z=39 and m/z=40 are found to be unchanged upon addition of a large amount of molecular hydrogen. Together with the previous studies on the photodissociation of C_3O_2 at 193 nm this strongly suggests that $C(^1D)$ atoms are not produced in a significant amount. To be cautious, all the experiments were conducted with a large excess of molecular hydrogen. In the following discussion reactions between $C(^1D)$ and the hydrocarbon reactants are neglected.

Figure 3 shows the photoionization spectrum measured at m/z=39. The solid red line is the photoionization spectrum of the propargyl radical (C_3H_3) obtained by Savee et al.[67] The very good match between the two spectra shows that propargyl is formed upon C_3O_2 photodissociation in the presence of ethylene. As indicated by previous H-atom branching ratio measurements and cross molecular beams

experiments,[14-16,19,20] the $C(^3P) + C_2H_4$ reaction is expected to solely produce the propargyl radical through an addition-elimination mechanism. Table S1 (see supplementary information) displays the predominant reactions resulting from the reaction system. Under these multiple collision conditions, the propargyl radical may be formed by the $C(^3P) + C_2H_4$ reaction as well as by the $C_2O + C_2H_3$ reaction. The C_2H_3 radical has an ionization energy of 8.25 eV and has been previously detected in similar experiments.[40] In Figure 2 the small signal at m/z=27 suggests that the vinyl radical is not formed in significant amount. In addition the rate coefficient for the $C_2O + C_2H_3$ is likely to be one order of magnitude slower than $C(^3P) + C_2H_4$ reaction (based on expected radical–radical kinetics of reactions with no barrier) and is therefore unlikely to contribute to the fast m/z=39 signal rise observed in Figure 5.

Figure 4 displays photoionization spectra of m/z=40. The red line is a fit to the spectrum using the experimental absolute spectra of allene[68] and methylaceytlene.[69] The best fit is within the 2-σ error bars and corresponds to branching fraction of 49% allene and 51% methylacetylene. The formation of C_3H_4 isomers (m/z = 40) upon irradiation of a C_3O_2/C_2H_4 gas mixture at 193 nm was also previously reported by Bayes et al.[70] As discussed by Kaiser et al.[19] the formation of the reaction adduct at m/z=40 upon attack of the triplet carbon atom onto the ethylene double bond does not lead to formation of the singlet C_3H_4 final products. The lifetime of the triplet C_3H_4 intermediate is expected to be on the order of, or shorter than, the rotational period of the molecules (0.5 ps along the C axis).[19] During this lifetime there will be a negligible number of collisions (<<1) between the triplet adduct and the He buffer gas. Crossing to the singlet surface is also predicted to be negligible.[19] The triplet adduct is therefore expected to rapidly dissociate to form the propargyl radical by H-loss with negligible contribution from stabilization of the triplet or singlet intermediate. The C_3H_4 isomers observed in Figures 1 and 2 are therefore likely to come from side reactions in the reaction flow.

Figure 5 shows the temporal trace of the C_3H_4-isomers (red squares) and the propargyl radical (blue circles) signals. The decay of the m/z=39 ion signal after the initial radical formation is due to the

propargyl self-reaction and reaction with the reactor tube walls. In the case of the closed-shell C_3H_4 products, the signal is stable after its formation, with a slight linear rise due to slight changes in laser fluence along the reactor tube. Within the experimental time resolution, both products are formed rapidly after irradiation of the gas mixture. The formation of propargyl radicals is likely to come from the $C(^3P)$ + C_2H_4 reaction whereas that of C_3H_4 isomers may be explained by either the C_2O + C_2H_4, or CH + C_2H_4 reaction (see Table S1). The C_2O radical is formed by photodissociation of the C_3O_2 precursor while the CH radical is formed by the C_2O + H reaction. At room temperature, the later reaction has a rate coefficient[59] of 3×10^{-11} cm^3 $molec^{-1}$ s^{-1} while CH + C_2H_4 has a rate coefficient of 2.84×10^{-10} cm^3 $molec^{-1}$ s^{-1}.[71] Using these rate coefficients, and estimating the ^1C_2O + C_3O_2 rate coefficient at 1×10^{-10} cm^3 $molec^{-1}$ s^{-1}, a simple kinetic model including C_2O + C_3O_2, C_2O + H, C + C_2H_4 and CH + C_2H_4 predicts a characteristic time for the rise of the C_3H_4 products of the order of 200 μs in agreement with the fast kinetic rise of m/z=40 in Figure 5. The C_3H_4 time-trace can be reproduced without including effects from the stabilization of the reaction adduct. This agrees with the short adduct lifetime discussed above.

Upon irradiation of the C_3O_2/ethylene mixture, signals at m/z=52 and m/z=42 are also observed when integrating the mass spectra over 40 ms of reaction time. Photoionization spectra of m/z=52 and m/z=42 identify them as vinylacetylene (C_4H_4) and ketene (H_2CCO, IE=9.6 eV)[72], respectively. Their formation kinetics is slower than that of the C_3H_4 isomers. Vinylacetylene is unlikely to come from the reaction of CH radicals with the C_3H_4 products as most CH radicals will be completely consumed by reactions with more abundant molecules such as C_2H_4 and C_3O_2 (see Table S1). The reaction of the CH radicals with the abundant C_3O_2 is expected to give C_2H radicals and two CO molecules.[61] The ethynyl radical can then react with ethylene to give vinylacetylene.[73] Alternatively the C_2O + C_3H_4 reaction may also lead to the formation of C_4H_4 by CO-loss. It is important to note that these products are the results of secondary and tertiary reactions and do not significantly contribute to the detected products at short

reaction time (see Figure 2). Ketene is likely formed by successive C_2O reactions with hydrocarbons and/or atomic hydrogen.

C(^{3}P) + propylene

According to the recent theoretical investigation of the C(^{3}P) reaction with propylene by Chin et al.[26] the main exothermic product channels are the following:

$C(^3P) + C_3H_6(X^1A')$	$\rightarrow$	$CH_3 + C_3H_3$	$\Delta H = -228.2$ kJ mol^{-1}
	$\rightarrow$	$H + C_4H_5$ ($H_2C–C\equiv C–CH_3$)	$\Delta H = -198.1$ kJ mol^{-1}
	$\rightarrow$	$H + C_4H_5$ ($H_2C=C–CH=CH_2$)	$\Delta H = -188.1$ kJ mol^{-1}
	$\rightarrow$	$H + C_4H_5$ ($HC\equiv C–CH–CH_3$)	$\Delta H = -186.8$ kJ mol^{-1}
	$\rightarrow$	$2H + C_4H_4$ ($HC\equiv C–CH=CH_2$)	$\Delta H = -8.4$ kJ mol^{-1}

Figure 6 displays the mass spectra obtained by photolysis of (a) propylene and (b) a mixture of C_3O_2 and propylene in helium. The data are recorded at 10 eV photon energy and integrated over the 0–1 ms reaction time window. By irradiating a mixture of propylene and helium in the absence of carbon suboxide, CH_3 (m/z=15), C_2H_3 (m/z=27), C_3H_3 (m/z=39) and C_3H_5 (m/z=41) are identified as products of propylene photolysis. At 193 nm, the absorption cross section of propylene is of the order of 3×10^{-19} cm^2 and its photodissociation also contributes to the negative signal at m/z=42.[74] Upon addition of carbon suboxide to the gas mixture the signal at m/z=39 increases significantly and signals at m/z=52 (C_4H_4), m/z=53 (C_4H_5) and m/z=54 (C_4H_6) appear. The main ion signals are detected at m/z=15, 27, 39, 41, 52, 53 and 54. Additional smaller signals are observed at m/z=51, 55, 56, 65, 66. Ion signal at m/z=40 is observed upon irradiation of propylene with no significant effect of C_3O_2 addition. In this case the C_3H_4 isomers may be formed by reaction of the propylene photoproducts such as $C_3H_5 + H$.[75]

Figure 7 presents the normalized time traces of some of the (a) odd and (b) even masses over the first 5 ms, integrated over the 8.5–10.5 eV energy range. The thick solid lines are (a) double exponential and (b) single exponential fits to the signals at m/z=53 and 40, respectively. In Figure 7 (a), the slower time constant in the double exponential is fixed to the value obtained by fitting the same data from 1 ms to 40 ms using a single exponential decay. Because the long time signal has contribution from dissociative ionization of an higher mass (see further) an ion offset is added to the fit and fixed to the signal value at 40 ms. The best fits return a pseudo first order rise of 2400 s^{-1} for m/z=40 and 5145 s^{-1} for m/z=53. Table S2 (see supplementary information) displays the main reactions expected to occur in the reaction flow upon irradiation of a C_3O_2/C_3H_6 mixture at 193 nm. The slower rise of the m/z=40 and 54 displayed in Figure 7 (b) compared to that of m/z=15, 39, and 53 suggests that they are formed by slower reactions than the $C(^3P)$ + propylene reaction or secondary processes such as C_2O, CH and C_2H reactions. The signal at m/z=52 is identified based on its photoionization spectrum as vinylacetylene (C_4H_4) likely formed by reaction of the C_2H radical with C_3H_6 (CH_3-loss channel).[73,76] Because the lifetime of the reaction adduct is expected to be very short,[24] products at m/z=54 are likely to be formed by the CH + C_3H_6 reaction.[43]

According to Table S2, C_4H_5 at m/z=53 may be formed by $C(^3P)$ + C_3H_6 or the unwanted C_2O + C_3H_5 reaction. We use the kinetic traces to distinguish between the two potential sources. Both the C_2O and C_3H_5 radicals are detected and are formed by 193 nm photolysis of C_3O_2 and C_3H_6, respectively. The C_2O + C_3H_5 reaction rate can be estimated to be of the order of 4×10^{-11} cm^3 s^{-1} based on barrierless radical–radical reactions. According to the C_3O_2 and C_3H_6 number densities and 193-nm absorption cross sections, both radicals are expected to be formed with similar number densities, on the order of 5×10^{12} cm^{-3}. The characteristic rise time of any reaction products is therefore expected to be 5 ms, which is much slower than the rise time of m/z=53 observed in Figure 7 (<500 μs). Based on this analysis, C_4H_5 + H are assigned as products of the $C(^3P)$ + C_3H_6 reaction.

The measurement of the C_4H_5/C_3H_3 branching ratio in the flow tube experiment is made difficult due to the high C_3H_6 193 nm-absorption cross section and high C_3H_3 formation quantum yield. In addition, the propargyl and methyl radicals may also be formed by the $C_2O + C_2H_3$ and $C_2H + C_3H_6$ reactions, respectively (Table S2). Based on similar kinetic arguments as for the C_4H_5 products, it is unlikely that these reaction contribute to the fast m/z=39 and m/z=15 rise displayed in Figure 7 (a). From Figure 7(a), propargyl and the C_4H_5 isomers have a very similar temporal profile. The product ratio can therefore be estimated directly from the ratio of the signal corrected by the relative ionization cross sections. Because the absolute ionization cross sections for the C_4H_5 isomers are unknown the ratio of the ion signals gives only an estimate of the H *vs*. CH_3 loss branching. The ratio of the m/z=39 and 53 signals from Figure 6 subtracted from the photodissociation spectrum acquired with only propylene and helium, and assuming similar ionization cross sections, suggest a 1:1 branching fraction.

Figure 8 displays the m/z=53 photoionization spectrum obtained by irradiating a C_3O_2 and propylene mixture a 193 nm. The data are integrated over the 0–40 ms time range and displayed from (a) 7.4 to 10.5 eV and (b) 7.4 to 8.25 eV. In panel (a) the vertical lines indicate the ionization energies of *i*-C_4H_5 (IE=7.55 eV),[77] and the methylpropargyl isomers (IE=7.94 eV for H_2CCCCH_3 and IE=7.95 eV for $HCCCHCH_3$),[77] all to their singlet ion state, as well as the ionization to the triplet ion state of H_2CCCCH_3 (IE=9.74 eV).[77] The ion signal observed above 7.5 eV and the ion onset at 7.9 eV suggest the presence *i*-C_4H_5 as well as one or two of the methylpropargyl isomers. Within the experimental photon energy resolution (40 meV) it is not possible to differentiate between the ionization of H_2CCCCH_3 or $HCCCHCH_3$. Additional ion signal onsets are observed at 8.25 eV and 9.5 eV. According to the calculated ionization energies of all the possible C_4H_5 isomers to their singlet or triplet ion states,[77] the transition from the ground neutral state to the triplet ion state of H_2CCCCH_3 has the closest energy (9.74 eV) to that of the observed feature at 9.5 eV. The poor Franck–Condon overlaps calculated for transition to H_2CCCCH_3 triplet state suggest that the observed ion signal about 9.5 eV is not due to H_2CCCCH_3

ionization. Alternatively the ionization signal above 9.6 eV could be due to the dissociative ionization of a higher mass, leading to a charged ion at m/z=53 and a neutral fragment. In this case the time profile of the daughter ion is that of the parent molecule. Figure 9 displays the temporal profile of m/z=53 integrated from 8.5 to 9.4 eV and from 9.5 to 10.5 eV. The difference between the temporal traces is constant with time, suggesting contribution from a stable species other than the C_4H_5 radical isomers. The photoion spectrum of m/z=54 can be reproduced with contributions from only two isomers: 1,3-butadiene and 1-butyne; there is no evidence for cyclic C_4H_6 isomers. Neither 1,3-butadiene nor 1-butyne will dissociate to give C_4H_5 over the experimental energy range.[46] The signal at photon energy higher than 9.5 eV is therefore likely to be mostly due to the dissociative ionization of a closed shell neutral whose parent ion corresponds to either 56 or 68. There is not enough information about the dissociative ionization of these molecules to conclusively assign the origin of the m/z=53 signal above 9.5 eV.

Figure 8b displays the m/z=53 photoionization spectrum over the 7.4–8.25 eV photon energy range together with the integrated Franck-Condon factor simulations for the *i*-C_4H_5 (dashed line) and the two methylpropargyl (dotted and dotted-dashed lines) isomers. The spectra for all the isomers are normalized to unity above 8.8 eV, where the simulated spectra are constant with photon energy. The thick red line is a fit to the experimental data up to 8.25 eV resulting in relative fractions of 1:4 for the *i*-C_4H_5 and methylpropargyl isomers, respectively, assuming equal ionization cross sections for all isomers. Because of the similarity of the methylpropargyl isomer spectra the fit is performed using only contribution from CH_3CCCH_2.

Figure 10 displays the m/z=53 photoionization spectra from the present experiments (circles) together with m/z=53 photoionization spectrum recorded in a low pressure (40 Torr) benzene flame (red line).[77] Similar photoionization spectra were recorded in cyclopentene, propyne, and allene flames.[77] Despite the large temperature difference, the very good overlap between the benzene flame spectrum and the present data strongly suggests that the C_4H_5 isomer distributions in the flow tube and in the flame are

similar. Hansen et al.[77] identified *i*-C_4H_5 and the methylpropargyl isomers as the main contributors to m/z=53 ion signal. The authors were not able to explain the ion threshold at 8.25 eV based on simulated photoionization spectra and detailed combustion modeling. Using the same fitting procedure as that described above, they infer an isomer distribution of 1:3, which is similar to that expected under thermal equilibrium at 1700 K (using computed enthalpies of formation).[49] At this temperature, the H_2CCCCH_3 isomer is twice as abundant as the $HCCCHCH_3$ isomer. At lower temperature, the equilibrium will shift toward the formation of the lowest energy isomer, H_2CCCCH_3. Close to room temperature under equilibrium conditions the contributions from *i*-C_4H_5 and $HCCCHCH_3$ are expected to be negligible. The detection of *i*-C_4H_5 in the flow tube experiment suggests that the measured m/z=53 ion spectrum in Figure 10 is not representative of a thermal equilibrium isomer distribution at 330 K.

Chin et al.[26] identified m/z=15, 39, 52, and 53 as the main products of the C(^{3}P) + propylene reaction under single collision conditions. They report a H:CH_3-loss channel ratio of 1:4 and a ratio of the sum of the methylpropargyl isomer densities over that of *i*-C_4H_5 of 1.4. The 1:4 branching ratio for H:CH_3-loss channels measured in crossed beams experiments differs from the 0.5 H-elimination branching ratio measured by Bergeat and Loison[17] under multiple collision conditions. The 1:1 normalized signal ratio between the m/z=39 and m/z=53 from Figure 6 agrees with the results from Bergeat and Loison at room temperature, with the caveat that we assume equal photoionization cross sections for these radicals. Assuming that the m/z=53 and m/z=39 are primary products from the C(^{3}P) + C_3H_6 reaction, the high collision energy in the crossed molecule beam experiments could account for the difference of H:CH_3.

Using RRKM calculations at about 16.7 kJ mol^{-1} collision energy,[26] Chin et al. predict a ratio of the sum of the methylpropargyl isomer densities over that of *i*-C_4H_5 of 1.2, which is close to their 1.4 experimental values. The difference from the ratio of 4 we measure in a flow tube close to room temperature is unlikely to come from pressure effects because the reaction adduct is expected to

decompose to the final products on a timescale much shorter than the collision rate.[24] This difference could suggest that the formation of the methylpropargyl isomers is favored at lower temperature. This dependence could come from the fact that the decomposition channels of the initial intermediates to methylpropargyl isomers have low or no barriers relatively to the formation of *i*-C_4H_5. However, such large changes in isomer distribution with temperature are usually not observed for very exothermic reactions where the average thermal energy represents only a very small fraction of the internal energy of the reaction intermediates. In addition, despite the multiple collision conditions, the short predicted lifetimes of the intermediates implies that these branching ratios results are unaffected by collisional energy transfer. The difference in isomer fraction between the two experiments could also be due to uncertainties when fitting the m/z=53 ion signal. In the case of the crossed beams experiments the $\Delta E/E$=4% (compared to $\Delta E/E$<1% for the present experiments) energy resolution does not allow the observation of the methylpropargyl isomers' ionization threshold.

The data displayed in Figures 8 allow the unambiguous identification of *i*-C_4H_5 and methylpropargyl isomers in the flow tube experiments. Large uncertainties still remain about the C_4H_5 isomer distribution mostly due to the unattributed signal above 8.2 eV in both the flame and flow tube experiments. Based on the previous identification this signal is likely to come from the ionization of either the *i*-C_4H_5 or the methylpropargyl isomers, although the Franck–Condon simulations do not predict it. Previous studies have shown that Franck–Condon overlap calculations fail at reproducing experimental ion spectra in the case of shape resonances.[78,79] The onset at 8.2 eV as well as the following structures (up to 9.4 eV) could therefore be due to auto-ionizing states of the neutral species at these energies. To our knowledge it is not possible to easily predict such features or to attribute them to one of the three considered isomers. If the ion signal at 8.2 eV is due to ionization of the methylpropargyl isomers, the relative branching ratios for the C_4H_5 isomers would be unchanged. However, if this feature were due to the ionization of *i*-C_4H_5, the isomer branching ratios would be greatly affected toward a much higher ratio

for *i*-C_4H_5. Such effect would affect the measured branching ratios in the flame, flow tube and crossed beams experiments the same way.

The detection of both *i*-C_4H_5 and methylpropargyl isomers from the C(^{3}P) + C_3H_6 reaction close to room temperature qualitatively agree with the previously accepted mechanisms inferred from single collision experiments and potential energy surfaces.[19,22,24] Once formed, the final products will rapidly be thermalized to the flow temperature by collisional quenching with the buffer gas. The reaction of the so formed C_4H_5 isomers with a H-atom present in the flow is barrier-less only in the case of the $HCCCHCH_3$ isomer. The reaction proceeds via the formation of the Z– or E–CH_3CHCCH_2 stereoisomers with no exit channels presenting energy barriers below the energy of the initial $HCCCHCH_3$ + H. The lowest energy product channel is the formation of C_3H_3 and CH_3 radicals. Such reaction would deplete the $HCCCHCH_3$ contribution toward formation of the propargyl and methyl radicals. H-assisted isomerization is therefore unlikely to contribute to the difference of isomer fraction between the crossed beams experiments and the flow tube experiments.

Astrophysical and combustion implications

***Titan and the interstellar medium*.** The kinetics of ground state carbon atoms, C(^{3}P), with ethylene and propylene has been shown to be fast down to very low temperature,[25] making these reactions of interest for the photochemical modeling of cold astrophysical environments rich in hydrocarbons. Titan, a satellite of Saturn, has been the subject of many studies in the last decade due to the successful Cassini mission, which revealed a far more complex chemistry than predicted[18,48,65,79,80] with neutral chemistry playing a central role.[45,49,62,79,80] Zhang et al.[3] identified the atomic neutral carbon emission CI line feature at 1657 Å ($2s^22p^13s^1\ ^3P_J - 2s^22p^2\ ^3P_J$) in the upper atmosphere of Titan using the Cassini Ultra-violet Imaging Spectrograph. CH + H[50] and CN + N[81] are the major sources of atomic carbon on Titan, while the reactions with C_2H_x hydrocarbons, mainly C_2H_2 and C_2H_4, are their most important loss processes, at least above 600 km[3]. Recently, Hébrard et al.,[49] pointing out that only a small fraction of all possible reactions

producing or involving C_3-compounds was included in previous photochemical models, reported an update of the photochemistry of C_3H_x in the stratosphere of Titan. Their study suggests that $C(^3P) + C_2H_2$ leads to the formation of C_3 and C_3H, while, $C(^3P) + C_2H_4$ forms essentially $C_3H_3 + H$, as inferred by Bergeat et al.,[16] and confirmed by the present study. The reaction of $C(^3P)$ with C_3H_6 however, plays a minor role in the formation of larger hydrocarbons on Titan due to the much lower molar fraction of propylene compared to acetylene in the atmosphere of Titan.[49] The situation is quite different for propylene in the interstellar medium. Due to its small dipole moment, it has been discovered only recently by Marcelino et al.[82] using the IRAM 30 m telescope in the giant Taurus Molecular Cloud 1 (TMC-1). An abundance relative to H_2 of $4x10^{-9}$, comparable to other abundant hydrocarbons in this cloud was derived from these observations, indicating the potential importance of propylene in the chemistry of the interstellar medium. The reactions involving propylene with abundant species such as atomic carbon, for instance, are therefore of importance in the chemical reaction network aiming to determine the abundance of molecular species in the interstellar medium.[83-85] The present study shows that even near room temperature, and likely below, the reaction of $C(^3P)$ atoms with propylene can form larger species such as C_4H_5 and may contribute to the formation of complex molecules in the interstellar medium.

Combustion environments: The detection of carbon atoms in flames is made very difficult due to the large absorption cross section of hydrocarbons at the VUV wavelengths used for laser induced fluorescence detection of $C(^3P)$. Ground state carbon has been detected in simple diffusion flames but the possible contribution from hydrocarbon photolysis by the excitation light has not been fully addressed.[4] In flames, carbon atoms could be formed by the CH + H reaction as suggested for cold environments. Although the reaction is thermodynamically favorable and occurs at fractions of the collision rate over the combustion temperature range,[46] this channel will remain minor because CH will preferentially react with more abundant fuel molecules. If formed, the carbon atoms will immediately react with the most abundant hydrocarbon molecules in the flame. Nevertheless, even a small amount of carbon atom self reaction could

also be responsible for part of the observed C_2 chemiluminescence.[5] The reaction of $C(^3P)$ with acetylene, ethylene and propylene would contribute to the formation of radicals such as C_3H, C_3H_3, CH_3 as well as C_4H_5, therefore participating in the propagation of the radical chemistry. The good match between the flame and flow tube C_4H_5 ion spectra could support a possible contribution from the $C(^3P) + C_3H_6$ reaction in combustion.

With the advent of interest in plasma assisted combustion, there is an important need to better understand the chemistry of the reactive species formed in such energy and carbon rich environments.[86] The neutral and ion chemical scheme initiated by plasma discharge in engines has been demonstrated to facilitate rapid combustion, thereby making it possible to use leaner mixtures, decreasing temperatures and hence NO_x production.[86] The carbon chemistry of these environments will be governed by fast ion and neutral reactions with the most abundant species. Carbon reactions may be able to compete with ion chemistry as long as carbon atoms are formed with a sufficiently high number density. Mass spectrometry experiments were able to detect carbon atoms in glow discharge plasmas[6] suggesting much higher concentrations than in combustion environments. The reaction of carbon atoms with the hydrocarbons present in high concentration will contribute to the neutral radical chemistry propagation and ultimately to the overall combustion process. More advanced computational models on the role of ion and neutral chemistry is required in order to better understand plasma assisted combustion phenomena.

Conclusions

We investigated the reaction of the ground state $C(^3P)$ with ethylene and propylene under multiple collision conditions at 332 K and 4 torr. Despite these multiple collision conditions, as long as reaction intermediates have short lifetimes relatively to the collision frequency, the observed product distribution is unaffected by collisional energy transfer. Carbon atoms are generated by 193 nm photodissociation of carbon suboxide in a large excess of molecular hydrogen in order to minimize any potential contributions

from C(^{1}D) reactions. Time- and energy-dependent photoionization spectra recorded with and without hydrogen as a C(^{1}D) scavenger indicate that only C(^{3}P) atoms are formed in the reaction flow. Time traces of the observed products were used to differentiate between primary and secondary reaction products and reaction kinetics considerations were used to discuss the origin of the detected products. In the case of C(^{3}P) + ethylene, the propargyl (C_3H_3) radical is detected as the major molecular reaction products in agreement with previous H-atom branching ratios and molecular beam experiments.

In the case of the C(^{3}P) + propylene reaction, the observed reaction channels are C_4H_5 + H and C_3H_3 + CH_3. The measured C_4H_5:C_3H_3 signal ratio from the present flow data is in agreement with the 1:1 H:CH_3-loss ratio from fast flow reactor H-atom detection results.[16,17] Photoionization spectra recorded at the mass of the C_4H_5 isomers show possible contamination from dissociative ionization of higher masses at energy above 9.5 eV. At lower energies, the C_4H_5 spectra are found to be almost identical to that recorded in a low pressure benzene flame.[77] The fit of the experimental data with integrated Franck–Condon factors gives a 1:4 relative distribution for the *i*-C_4H_5 isomer relatively to the sum of both methylpropargyl isomers. The resemblance between the flame and flow tube data could indicate that the photoionization spectrum of the *i*-C_4H_5 isomer displays a strong shape resonance features above its ionization threshold and eventually around the ionization energy of the methylpropargyl isomers. If true, the contribution from the methylpropargyl isomers to the overall isomer distribution would be overestimated in the flow tube, flame and cross-molecular beam experiments.

The good match between the flow tube and the flame spectra at m/z=53 suggests that C_4H_5 isomers are likely to play a significant role in combustion chemistry. Carbon atoms are also present in plasmas where they will contribute to the molecular growth. For these reasons the C(^{3}P) + C_3H_6 reaction needs to be studied over a wide range of experimental conditions, included collisional environments. The branching ratios measured in crossed beam experiments were so far the only available experimental data for the C(^{3}P) + C_3H_6 reaction. The flow tube data extend the previous results to a much wider range of

experimental conditions more relevant for combustion and plasma chemistry. Under multiple collision conditions, the present experiments suggest the formation methyl and propargyl radicals in non-negligible amounts alongside both *i*-C_4H_5 and methylpropargyl isomers. Suggested branching ratios for computational model are 1:4 for the *i*-C_4H_5:methylpropargyl isomers. Further computational studies are required in order to determine the effect of these branching ratios on the outcome of chemical models.

ACKNOWLEDGMENTS

The Rennes team acknowledges support from the Agence Nationale de la Recherche, contract ANR-11-BS04-024-CRESUSOL-01, the French INSU/CNRS Program "Physique et Chimie du Milieu Interstellaire" (PCMI), the Institut National de Physique (INP CNRS), the Région Bretagne and the Université de Rennes 1. S.D.L.P. acknowledges financial support from the Institut Universitaire de France. F.G. And R.K.A.K. acknowledge founding by the West Virginia University (startup package) for supply and personal support and the Petroleum Research Funds (PRF# 53105-DNI6) for post-doctoral support (R.K.A.K.). We thank Mr. Howard Johnsen and Dr. John Savee for technical support of this experiment. We also thank Dr. Craig A. Taatjes for his comments on the early draft of the manuscript and Dr. Jean-Christophe Loison for his help with the Franck-Condon factor calculations and valuable discussions about secondary reactions. We also thank Dr. Doug Taube for his help and advise during the carbon suboxide synthesis. D.L.O. and the instrumentation for this work are supported by the Division of Chemical Sciences, Geosciences, and Biosciences, the Office of Basic Energy Sciences, the U. S. Department of Energy. Sandia is a multi-program laboratory operated by Sandia Corporation, a Lockheed Martin Company, for the National Nuclear Security Administration under contract DE-AC04-94-AL85000. This research used resources of the Advanced Light Source, a DOE Office of Science User Facility, which is supported by the Direct, Office of Science, Office of Basic Energy Sciences, the U.S. Department of Energy under contract DE-AC02-05CH11231 at Lawrence Berkeley National Laboratory.

References

1. J. G. Ingalls, T. M. Bania and J. M. Jackson, *Astrophys. J.*, 1994, **431**, L139-L142.

2. W. Van der Veen, P. J. Huggins and H. E. Matthews, *Astrophys. J.*, 1998, **505**, 749-755.

3. X. Zhang, J. M. Ajello and Y. L. Yung, *Astrophys. J. Lett.*, 2010, **708**, L18-L21.

4. M. Alden, P. E. Bengtsson and U. Westblom, *Opt. Commun.*, 1989, **71**, 263-268.

5. C. S. T. Marques, L. H. Benvenutti and C. A. Bertran, *J. Braz. Chem. Soc.*, 2006, **17**, 302-315.

6. A. E. Belikov, S. Z. Sakhapov, M. A. Smith and G. Tikhonov, *J. Eng. Thermophys.*, 2011, **20**, 42-54.

7. J. Benedikt, M. Wisse, R. V. Woen, R. Engeln and M. C. M. van de Sanden, *J. Appl. Phys.*, 2003, **94**, 6932-6938.

8. B. W. Yu and S. L. Girshick, *J. Appl. Phys.*, 1994, **75**, 3914-3923.

9. M. A. Malik, D. Hughes, A. Malik, S. Xiao and K. H. Schoenbach, *Plasma Chem. Plasma Pocess.*, 2013, **33**, 271-279.

10. N. Haider and D. Husain, *Int. J. Res. Phys. Chem. Chem. Phys.*, 1992, **176**, 133-150.

11. N. Haider and D. Husain, *Ber. Bunsen-Ges. Phys. Chem. Chem. Phys.*, 1993, **97**, 571-577.

12. D. Chastaing, S. D. Le Picard, I. R. Sims and I. W. M. Smith, *Astron. Astrophys.*, 2001, **365**, 241-247.

13. D. Chastaing, S. D. Le Picard, I. R. Sims, I. W. M. Smith, W. D. Geppert, C. Naulin and M. Costes, *Chem. Phys. Lett.*, 2000, **331**, 170-176.

14. W. D. Geppert, C. Naulin, M. Costes, G. Capozza, L. Cartechini, P. Casavecchia and G. G. Volpi, *J. Chem. Phys.*, 2003, **119**, 10607-10617.

15. R. I. Kaiser and A. M. Mebel, *Inter. Rev. Phys. Chem.*, 2002, **21**, 307-356.

16. A. Bergeat and J. C. Loison, *Phys. Chem. Chem. Phys.*, 2001, **3**, 2038-2042.

17. J. C. Loison and A. Bergeat, *Phys. Chem. Chem. Phys.*, 2004, **6**, 5396-5401.

18. T. E. Cravens, I. P. Robertson, J. H. Waite, R. V. Yelle, W. T. Kasprzak, C. N. Keller, S. A. Ledvina, H. B. Niemann, J. G. Luhmann, R. L. McNutt, W. H. Ip, V. De La Haye, I. Mueller-Wodarg, J. E. Wahlund, V. G. Anicich and V. Vuitton, *Geophys. Res. Lett.*, 2006, **33**, L07105: 1-4.

19. R. I. Kaiser, Y. T. Lee and A. G. Suits, *J. Chem. Phys.*, 1996, **105**, 8705-8720.

20. C. H. Chin, W. K. Chen, W. J. Huang, Y. C. Lin and S. H. Lee, *J. Phys. Chem. A*, 2012, **116**, 7615-7622.

21. R. I. Kaiser, T. L. Nguyen, T. N. Le and A. M. Mebel, *Astrophys. J.*, 2001, **561**, 858-863.

22. T. N. Le, H. Y. Lee, A. M. Mebel and R. I. Kaiser, *J. Phys. Chem. A*, 2001, **105**, 1847-1856.

23. A. M. Mebel, W. M. Jackson, A. H. H. Chang and S. H. Lin, *J. Am. Chem. Soc.*, 1998, **120**, 5751-5763.

24. R. I. Kaiser, D. Stranges, H. M. Bevsek, Y. T. Lee and A. G. Suits, *J. Chem. Phys.*, 1997, **106**, 4945-4953.

25. D. Chastaing, P. L. James, I. R. Sims and I. W. M. Smith, *Phys. Chem. Chem. Phys.*, 1999, **1**, 2247-2256.

26. C. H. Chin, W. K. Chen, W. J. Huang, Y. C. Lin and S. H. Lee, *Icarus*, 2013, **222**, 254-262.

27. F. Goulay, D. L. Osborn, C. A. Taatjes, P. Zou, G. Meloni and S. R. Leone, *Phys. Chem. Chem. Phys.*, 2007, **9**, 4291-4300.

28. F. Goulay, A. J. Trevitt, G. Meloni, T. M. Selby, D. L. Osborn, C. A. Taatjes, L. Vereecken and S. R. Leone, *J. Am. Chem. Soc.*, 2009, **131**, 993-1005.

29. C. A. Taatjes, N. Hansen, D. L. Osborn, K. Kohse-Hoeinghaus, T. A. Cool and P. R. Westmoreland, *Phys. Chem. Chem. Phys.*, 2008, **10**, 20-34.

30. C. A. Taatjes, D. L. Osborn, T. M. Selby, G. Meloni, A. J. Trevitt, E. Epifanovsky, A. I. Krylov, B. Sirjean, E. Dames and H. Wang, *J. Phys. Chem. A*, 2010, **114**, 3355-3370.

31. O. Welz, J. D. Savee, D. L. Osborn, S. S. Vasu, C. J. Percival, D. E. Shallcross and C. A. Taatjes, *Science*, 2012, **335**, 204-207.

32. D. L. Osborn, P. Zou, H. Johnsen, C. C. Hayden, C. A. Taatjes, V. D. Knyazev, S. W. North, D. S. Peterka, M. Ahmed and S. R. Leone, *Rev. Sci. Instrum.*, 2008, **79**, 104103: 1-10.

33. I. Hahndorf, Y. T. Lee, R. I. Kaiser, L. Vereecken, J. Peeters, H. F. Bettinger, P. R. Schreiner, P. V. Schleyer, W. D. Allen and H. F. Schaefer, *J. Chem. Phys.*, 2002, **116**, 3248-3262.

34. R. I. Kaiser, X. Gu, F. Zhang and P. Maksyutenko, *Phys. Chem. Chem. Phys.*, 2012, **14**, 575-588.

35. R. I. Kaiser, T. N. Le, T. L. Nguyen, A. M. Mebel, N. Balucani, Y. T. Lee, F. Stahl, P. V. Schleyer and H. F. Schaefer, *J. Chem. Soc., Faraday Trans.*, 2001, **119**, 51-66.

36. S. B. Morales, C. J. Bennett, S. D. Le Picard, A. Canosa, I. R. Sims, B. J. Sun, P. H. Chen, A. H. H. Chang, V. V. Kislov, A. M. Mebel, X. Gu, F. Zhang, P. Maksyutenko and R. I. Kaiser, *Astrophys. J.*, 2011, **742**, 1-10.

37. N. Balucani, F. Leonori, A. Bergeat, R. Petrucci and P. Casavecchia, *Phys. Chem. Chem. Phys.*, 2011, **13**, 8322-8330.

38. P. Casavecchia, N. Balucani, L. Cartechini, G. Capozza, A. Bergeat and G. G. Volpi, *J. Chem. Soc., Faraday Trans.*, 2001, **119**, 27-49.

39. F. Goulay, S. Soorkia, G. Meloni, D. L. Osborn, C. A. Taatjes and S. R. Leone, *Phys. Chem. Chem. Phys.*, 2011, **13**, 20820-20827.

40. F. Goulay, A. J. Trevitt, J. D. Savee, J. Bouwman, D. L. Osborn, C. A. Taatjes, K. R. Wilson and S. R. Leone, *J. Phys. Chem. A*, 2012, **116**, 6091-6106.

41. J. F. Lockyear, O. Welz, J. D. Savee, F. Goulay, A. J. Trevitt, C. A. Taatjes, D. L. Osborn and S. R. Leone, *J. Phys. Chem. A*, 2013, **117**, 11013-11026.

42. T. M. Selby, G. Meloni, F. Goulay, S. R. Leone, A. Fahr, C. A. Taatjes and D. L. Osborn, *J. Phys. Chem. A*, 2008, **112**, 9366-9373.

43. A. J. Trevitt, M. B. Prendergast, F. Goulay, J. D. Savee, D. L. Osborn, C. A. Taatjes and S. R. Leone, *J. Phys. Chem. A*, 2013, **117**, 6450-6457.

44. C. A. Taatjes, N. Hansen, D. L. Osborn, K. Kohse-Hoinghaus, T. A. Cool and P. R. Westmoreland, *Phys. Chem. Chem. Phys.*, 2008, **10**, 20-34.

45. R. V. Yelle, V. Vuitton, P. Lavvas, S. J. Klippenstein, M. A. Smith, S. M. Horst and J. Cui, *J. Chem. Soc., Faraday Trans.*, 2010, **147**, 31-49.

46. NIST, 2005, Standard Reference Database Number 69, NIST Chemistry WebBook, National Institute of Standards and Technology, Gaithersburg MD, 20899 (http://webbook.nist.gov).

47. Y. J. Ma, A. F. Nagy, T. E. Cravens, I. V. Sokolov, K. C. Hansen, J. E. Wahlund, F. J. Crary, A. J. Coates and M. K. Dougherty, *J. Geophys. Res.*, 2006, **111**, A05207: 1-14.

48. A. J. Coates, F. J. Crary, G. R. Lewis, D. T. Young, J. H. Waite and E. C. Sittler, *Geophys. Res. Lett.*, 2007, **34**, L22103: 1-6.

49. E. Hebrard, M. Dobrijevic, J. C. Loison, A. Bergeat, K. M. Hickson and F. Caralp, *Astron. Astrophys.*, 2013, **552**, A132: 1-21.

50. R. van Harrevelt, M. C. van Hemert and G. C. Schatz, *J. Chem. Phys.*, 2002, **116**, 6002-6011.

51. D. J. Anderson and R. N. Rosenfeld, *J. Chem. Phys.*, 1991, **94**, 7857-7867.

52. K. Bayes, *J. Am. Chem. Soc.*, 1961, **83**, 3712-3713.

53. J. McFarlane, J. C. Polanyi, J. G. Shapter and J. M. Williamson, *J. Photochem. Photobio. A*, 1989, **46**, 139-158.

54. H. Okabe, *Photochemistry of Small Molecules* John Wiley & Sons, New York, 1978.

55. Y. Osamura, K. Nishimoto, S. Yamabe and T. Minato, *Theor. Chim. Acta*, 1979, **52**, 257-265.

56. J. L. Roebber, J. C. Larrabee and R. E. Huffman, *J. Chem. Phys.*, 1967, **46**, 4594-4600.

57. D. Chastaing, S. D. Le Picard and I. R. Sims, *J. Chem. Phys.*, 2000, **112**, 8466-8469.

58. W. Bauer, R. Meuser and K. H. Becker, *J. Photochem.*, 1984, **24**, 99-102.

59. W. Bauer, K. H. Becker and R. Meuser, *Ber. Bunsen-Ges. Phys. Chem. Chem. Phys.*, 1985, **89**, 340-341.

60. C. Y. R. Wu, F. Z. Chen and D. L. Judge, *J. Gephys. Res.*, 2004, **109**, E07S15: 1-7.

61. K. Sato, N. Ishida, T. Kurakata, A. Iwasaki and S. Tsunashima, *Chem. Phys.*, 1998, **237**, 195-204.

62. V. Vuitton, R. V. Yelle, P. Lavvas and S. J. Klippenstein, *Astrophys. J.*, 2012, **744**, 1-7.

63. D. Husain and A. N. Young, *J. Chem. Soc. Faraday Trans.*, 1975, **71**, 525-531.

64. Y. Wu, C. F. Zhang, J. W. Cao and W. S. Bian, *J. Phys. Chem. A*, 2014, **118**, 4235-4242.

65. V. Vuitton, R. V. Yelle and M. J. McEwan, *Icarus*, 2007, **191**, 722-742.

66. J. Cui, R. V. Yelle, V. Vuitton, J. H. Waite, W. T. Kasprzak, D. A. Gell, H. B. Niemann, I. C. F. Muller-Wodarg, N. Borggren, G. G. Fletcher, E. L. Patrick, E. Raaen and B. A. Magee, *Icarus*, 2009, **200**, 581-615.

67. J. D. Savee, S. Soorkia, O. Welz, T. M. Selby, C. A. Taatjes and D. L. Osborn, *J. Chem. Phys.*, 2012, **136**, 134307: 1-10.

68. B. Yang, J. Wang, T. A. Cool, N. Hansen, S. Skeen and D. L. Osborn, *Int. J. Mass Spectrom. Ion Proc.*, 2012, **309**, 118-128.

69. T. A. Cool, K. Nakajima, T. A. Mostefaoui, F. Qi, A. McIlroy, P. R. Westmoreland, M. E. Law, L. Poisson, D. S. Peterka and M. Ahmed, *J. Chem. Phys.*, 2003, **119**, 8356-8365.

70. K. D. Bayes, *J. Am. Chem. Soc.*, 1962, **84**, 4077-4080.

71. H. Thiesemann, E. P. Clifford, C. A. Taatjes and S. J. Klippenstein, *J. Phys. Chem. A*, 2001, **105**, 5393-5401.

72. F. Goulay, A. Derakhshan, E. Maher, A. J. Trevitt, J. D. Savee, A. M. Scheer, D. L. Osborn and C. A. Taatjes, *Phys. Chem. Chem. Phys.*, 2013, **15**, 4049-58.

73. J. Bouwman, F. Goulay, S. R. Leone and K. R. Wilson, *J. Phys. Chem. A*, 2012, **116**, 3907-3917.

74. A. Fahr and A. Nayak, *Chem. Phys.*, 1996, **203**, 351-358.

75. M. A. Hanninglee and M. J. Pilling, *Int. J. Chem. Kinet.*, 1992, **24**, 271-278.

76. T. A. Cool, J. Wang, K. Nakajima, C. A. Taatjes and A. McIlroy, *Int. J. Mass Spectrom. Ion Proc.*, 2005, **247**, 18-27.

77. N. Hansen, S. J. Klippenstein, C. A. Taatjes, J. A. Miller, J. Wang, T. A. Cool, B. Yang, R. Yang, L. X. Wei, C. Q. Huang, F. Qi, M. E. Law and P. R. Westmoreland, *J. Phys. Chem. A*, 2006, **110**, 3670-3678.

78. H. Xu, U. Jacovella, B. Ruscic, S. T. Pratt and R. R. Lucchese, *J. Chem. Phys.*, 2012, **136**, 154303: 1-10.

79. V. Vuitton, R. V. Yelle and J. Cui, *J. Gephys. Res.*, 2008, **113**, E05007: 1-18.

80. V. Vuitton, R. V. Yelle and P. Lavvas, *Phil. Trans. Royal. Soc. A*, 2009, **367**, 729-741.

81. J. Daranlot, U. Hincelin, A. Bergeat, M. Costes, J. C. Loison, V. Wakelam and K. M. Hickson, *Proc. Natl. Acad. Sci. U. S. A.*, 2012, **109**, 10233-10238.

82. N. Marcelino, J. Cernicharo, M. Agundez, E. Roueff, M. Gerin, J. Martin-Pintado, R. Mauersberger and C. Thum, *Astrophys. J.*, 2007, **665**, L127-L130.

83. M. Agundez and V. Wakelam, *Chem. Rev.*, 2013, **113**, 8710-8737.

84. J. M. C. Rawlings, D. A. Williams, S. Viti and C. Cecchi-Pestellini, *Mon. Not. R. Astron. Soc.*, 2013, **436**, L59-L63.

85. J. M. C. Rawlings, D. A. Williams, S. Viti, C. Cecchi-Pestellini and W. W. Duley, *J. Chem. Soc., Faraday Trans.*, 2014, **168**, 369-388.

86. A. Y. Starikovskii, *Proc. Comb. Inst.*, 2005, **30**, 2405-2417.

Figures

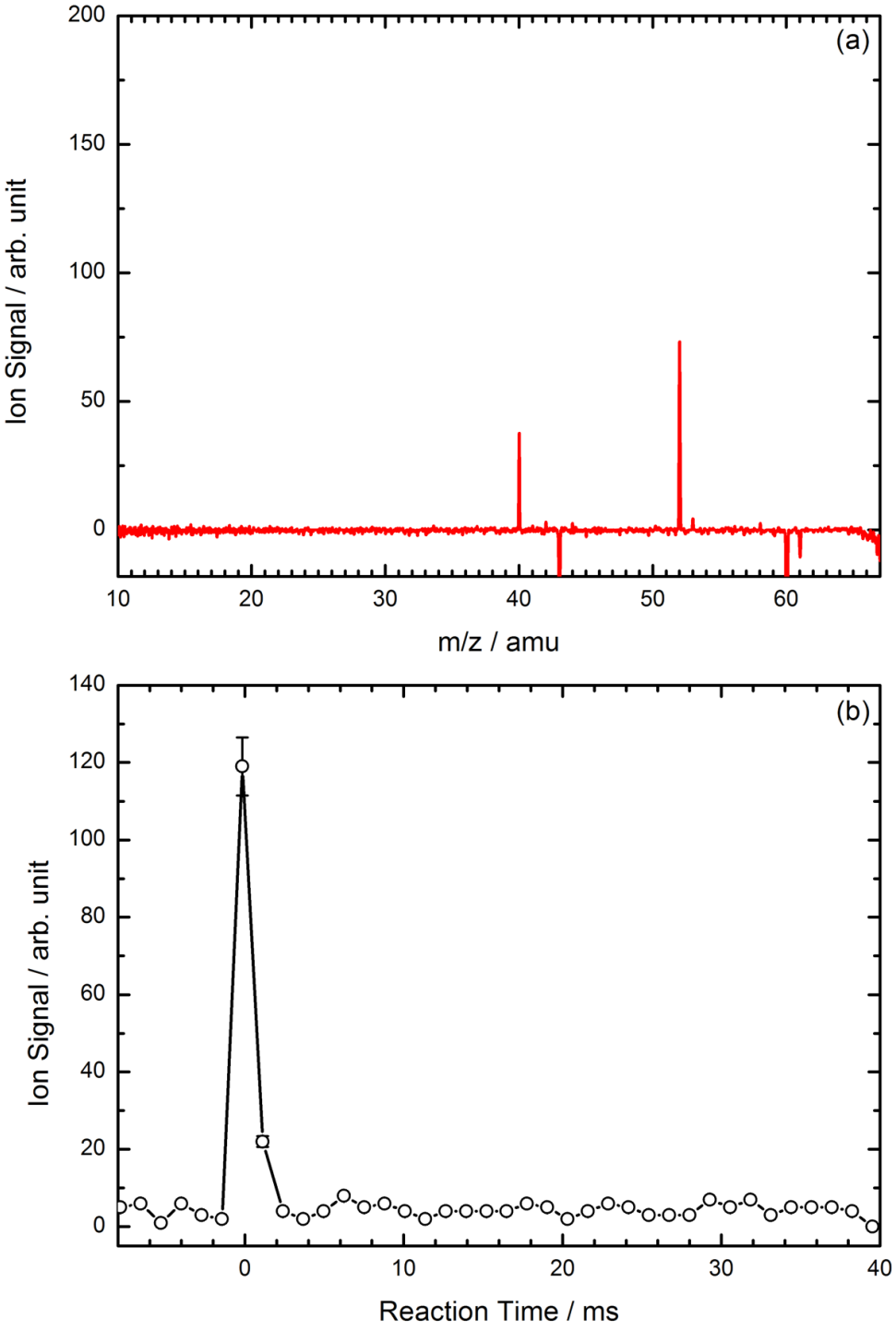

Figure 1: (a) Mass spectrum integrated over the 0–1 ms time range and (b) m/z=40 kinetic trace recorded at 11.3 eV photon energy upon irradiation of C_3O_2 in helium.

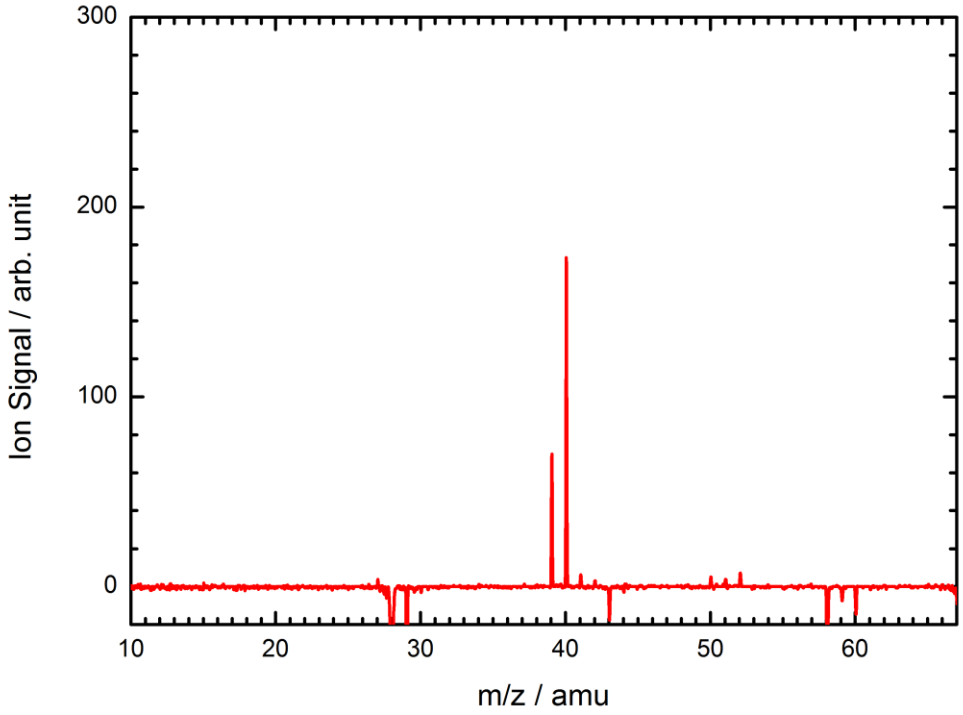

Figure 2: Mass spectrum obtained by photolysis of a C_3O_2 and ethylene mixture in helium, at 10.7 eV photon energy, integrated over the 0–1 ms time range.

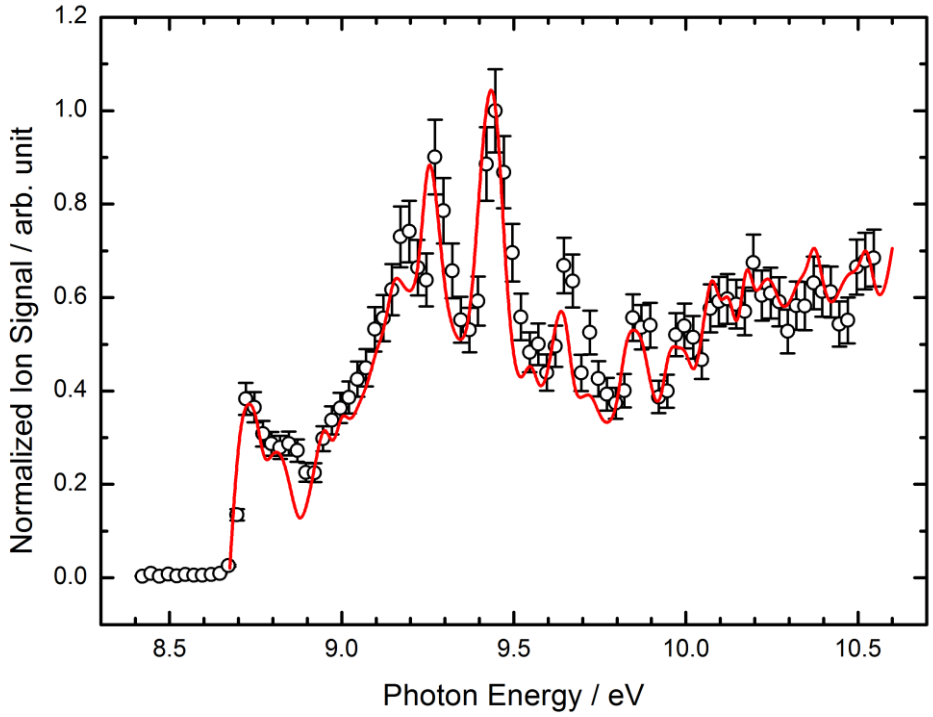

Figure 3: Photoion signal at m/z 39 ion (open circles) integrated over the 0–40 ms time range obtained by photolysis of a C_3O_2 and ethylene mixture in helium together with the absolute spectrum (solid red line) of the propargyl radical (C_3H_3) obtained by Savee et al.[51]

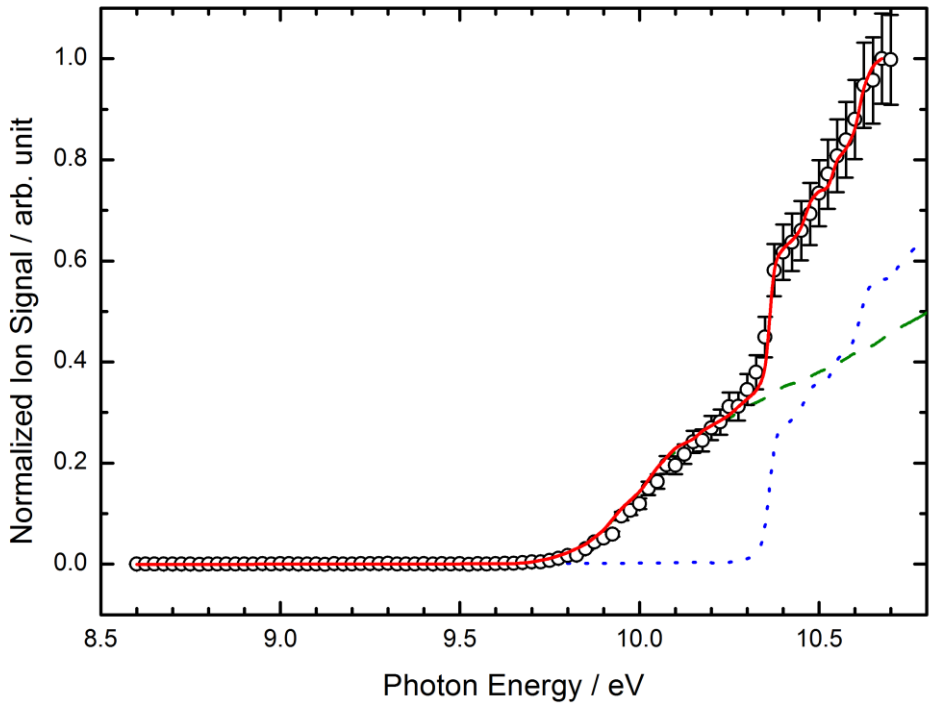

Figure 4: Photoion signal at m/z = 40 (open circles) obtained by photolysis of a C_3O_2 and ethylene mixture in helium. The red solid line is a fit to the data using the absolute photoion spectra of allene (green dashed line) from Yang et al.[52] and methylaceytlene (blue point line) from Cool et al.[53] The best fit to the data is obtained for 49% allene and 51% methylacetylene.

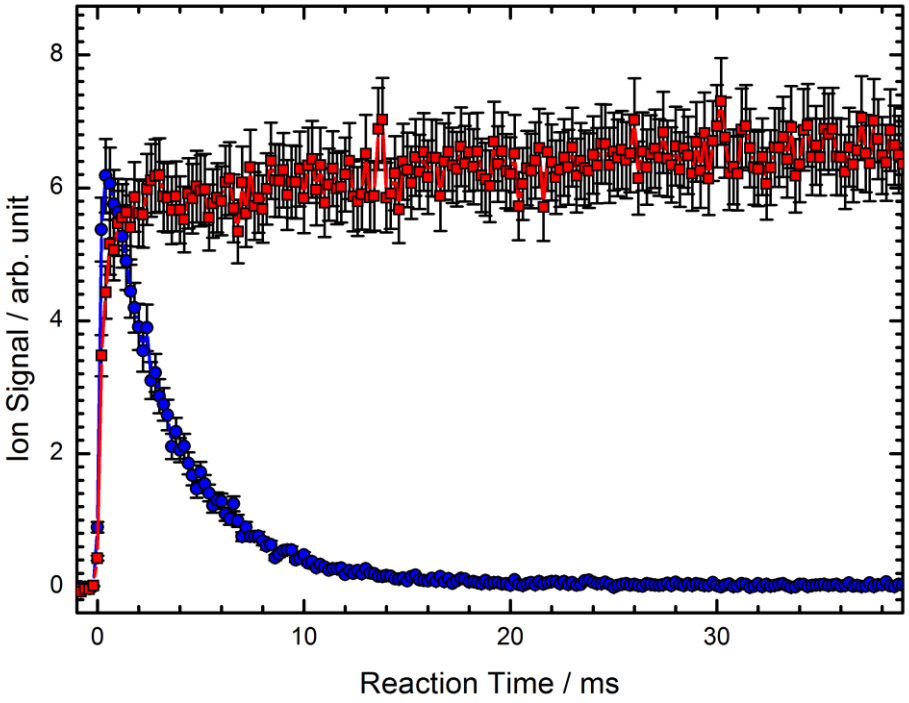

Figure 5: Kinetic traces of C_3H_4 isomers (red squares) and propargyl radical C_3H_3 (blue circles) integrated over the 8.6-10.6 eV photon energy range obtained by photolysis of a C_3O_2 and ethylene mixture in helium. Error bars are derived from Poisson counting statistics

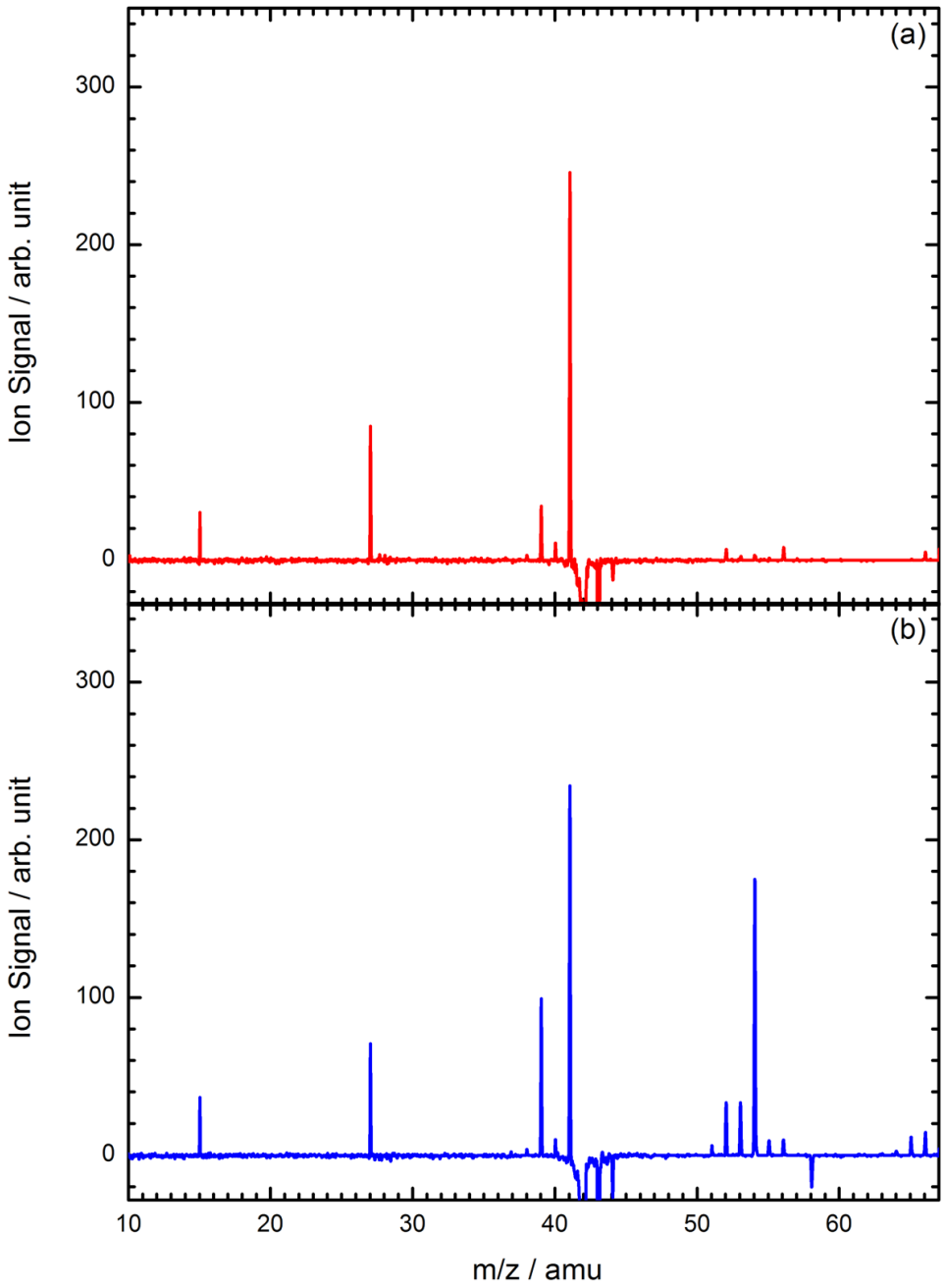

Figure 6: Mass spectra obtained by 193-nm photolysis of (a) propylene in helium and (b) a mixture of propylene and C_3O_2 in helium, recorded at 10 eV photon energy and integrated over the 0–1 ms time range.

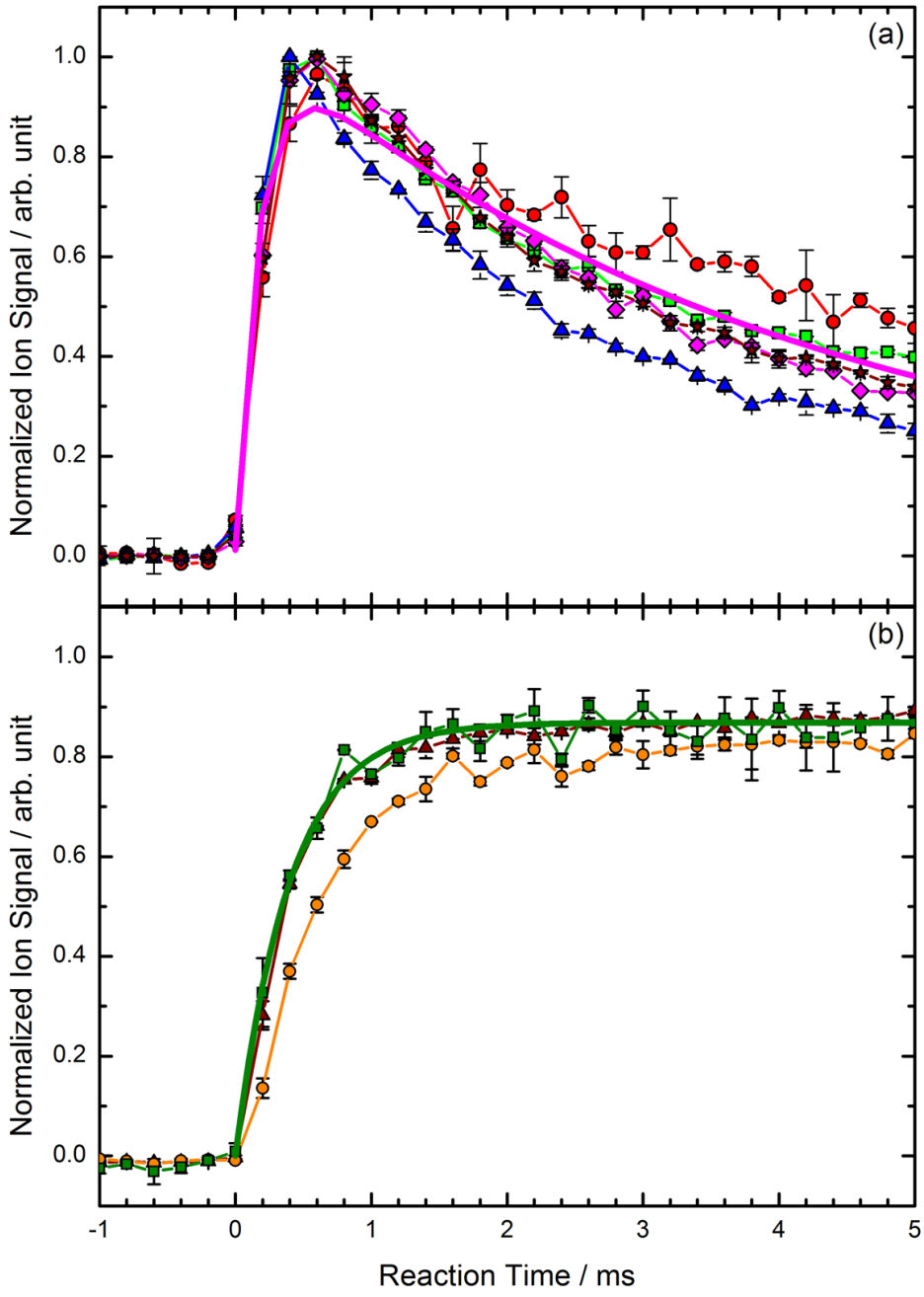

Figure 7: Normalized kinetic traces obtained by photolysis of a C_3O_2 and propylene mixture in helium of (a) mass 15 (red circles), 27 (blue triangles), 39 (brown stars), 41 (green squares) and 53 (purple diamonds) and (b) mass 40 (green squares), 52 (orange circles) and 54 (brown triangles) integrated over the 8.5–10.5 eV energy photon range. The thick pink line in (a) is a double exponential fit to m/z=53. The thick green line in (b) is a single exponential fit to m/z=40.

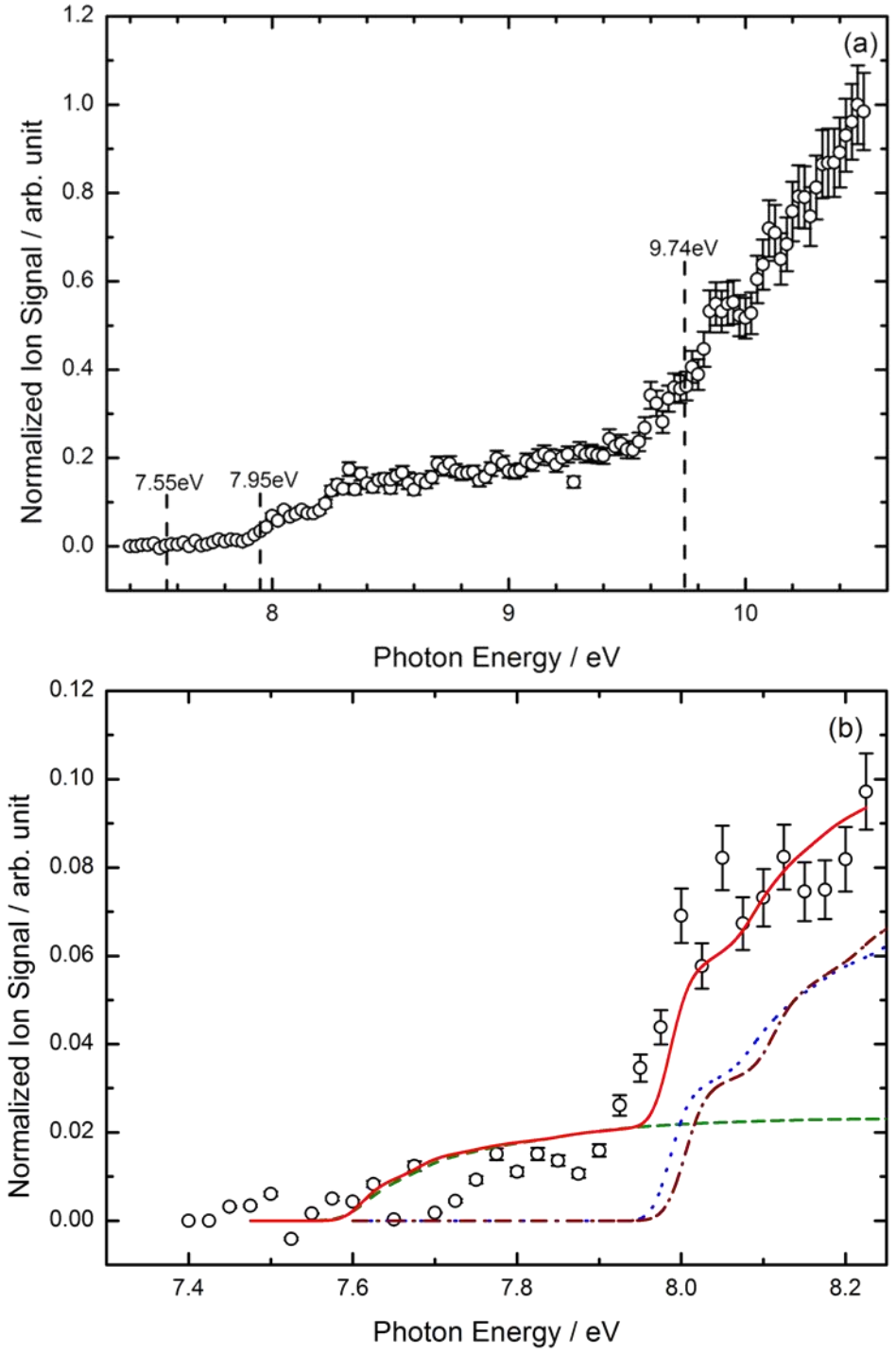

Figure 8: Photoionization spectrum of m/z=53 obtained by photolysis of a C_3O_2 and propylene mixture in helium integrated over the 0–40 ms time range and displayed from (a) 7.4 to 10.5 eV and (b) 7.4 to 8.25 eV photon energy. The vertical dashed lines in panel (a) correspond to the photoionization of *i*-C_4H_5, methylpropargyl isomers to their singlet ion state and to the triplet ion state of H_2CCCCH_3. The lines in panel (b) are the integrated Franck-Condon factor simulations for *i*-C_4H_5 (green dashed line) and the two methylpropargyl (blue

dotted and brown dashed dotted lines) isomers. The thick red line is a fit to the experimental data up to 8.25 eV yielding a 1:4 ratio of *i*-C_4H_5 : methylpropargyl isomers.

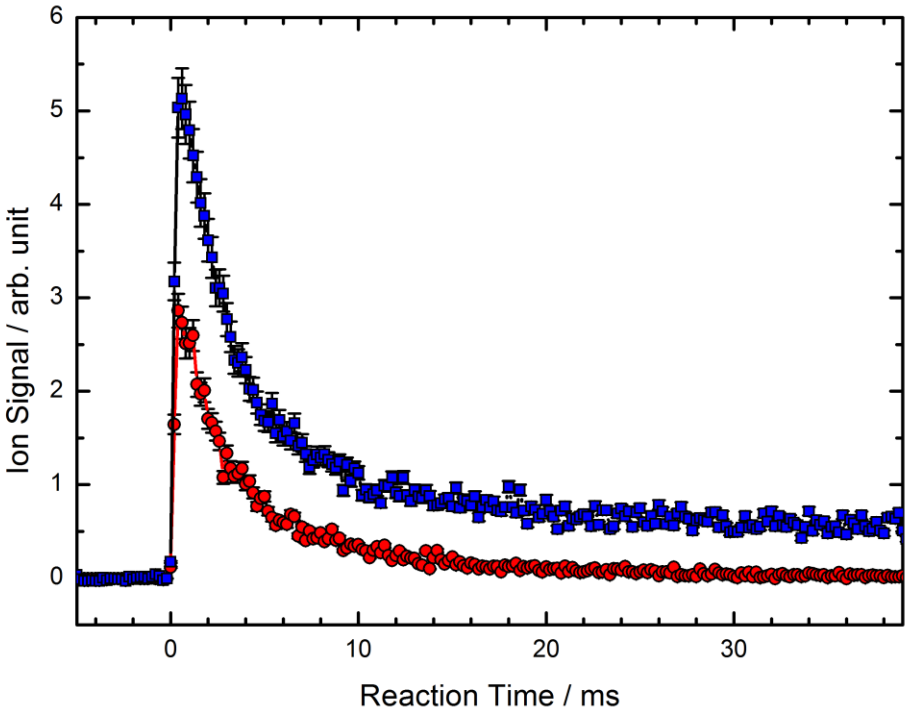

Figure 9: Kinetic traces of m/z=53 integrated from 8.5 to 9.4 eV photon energy (red circles) and from 9.5 to 10.5 eV (blue squares).

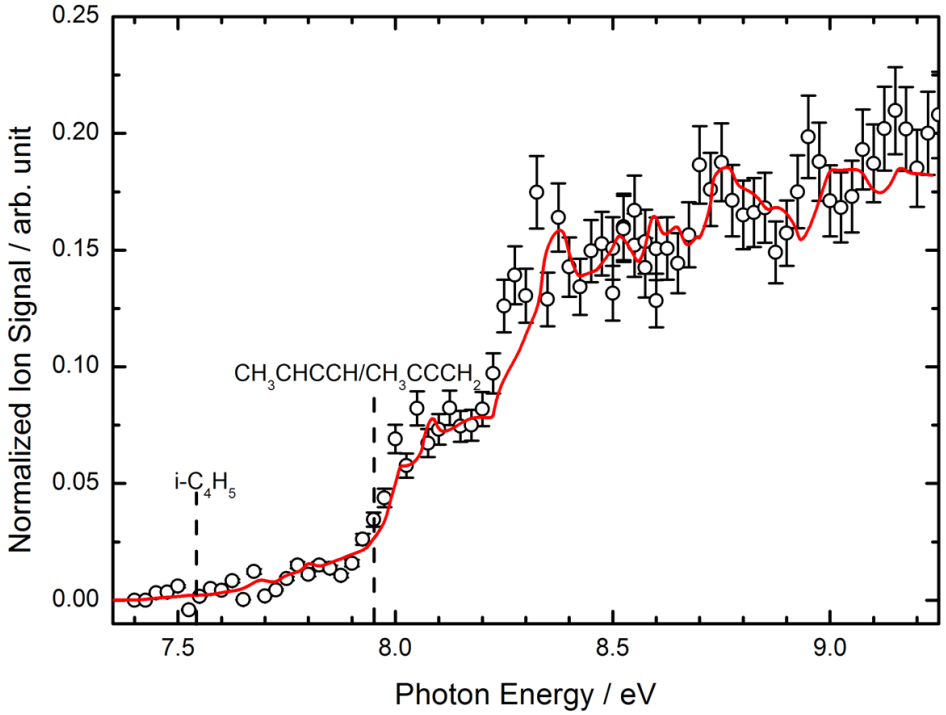

Figure 10: Photoionization spectrum of m/z=53 from the C(^{3}P) + C_3H_6 reaction integrated over 40 ms after lasher shot and displayed from 7.4 to 9.2 eV photon energy. The red line is m/z=53 photoionization spectrum recorded in a low pressure (40 Torr) benzene flame.[60]